analytical chemistry

pubs.acs.org/ac Article

Magnetic Susceptibility-Based Protein Detection Using Magnetic Levitation

Sena Yaman and H. Cumhur Tekin*

Cite This: *Anal. Chem.* 2020, 92, 12556−12563 Read Online

ACCESS | Metrics & More | Article Recommendations | Supporting Information

ABSTRACT: Magnetic levitation, which is a magnetic phenomenon of levitating particles suspended in a paramagnetic liquid under a nonuniform magnetic field, is a powerful tool for determining densities and magnetic properties of micro- and nanoparticles. The levitation height of particles in the magnetic field depends on the magnetic susceptibility and density difference between the object and the surrounding liquid. Here, we developed a magnetic susceptibility-based protein detection scheme in a low-cost and miniaturized magnetic levitation setup consisting of two opposing magnets to create a gradient of a magnetic field, a glass capillary channel to retain the sample, and two side mirrors to monitor inside the channel. The method includes the use of polymeric microspheres as mobile assay surfaces and magnetic nanoparticles as labels. The assay was realized by capturing the target protein to the polymer microspheres. Then, magnetic nanoparticles were attached onto the resulting microsphere−protein complex, creating a significant difference in the magnetic properties of polymer microspheres compared to those without protein. The change in the magnetic properties caused a change in the levitation height of the microspheres. The levitation heights and their distribution were then correlated to the amount of target proteins. The method enabled a detection limit of ∼110 fg/mL biotinylated bovine serum albumin in serum. With the sandwich immunoassay developed for mouse immunoglobulin G, detection limits of 1.5 ng/mL and >10 ng/mL were achieved in buffer and serum, respectively. This approach sensed the minute changes in the volume magnetic susceptibility of the microspheres with a resolution of 4.2×10^{-8} per 1 μm levitation height change.

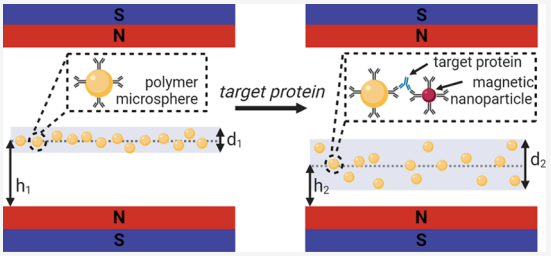

Protein biomarkers in blood serve as molecular signatures of complex diseases such as cancer,[1−3] cardiovascular disorders,[4] and other pathological situations.[5,6] Hence, sensitive and rapid protein detection provides valuable information about the presence and course of a disease that could improve the survival rate of patients. However, a biomarker may be present at very low levels (e.g., sub-ng/mL) in the blood, which requires large volumes of samples and long processing time for classical biomarker analysis techniques (e.g., enzyme-linked immunosorbent assay (ELISA)). In addition, the lack of portability hinders the applicability of traditional techniques in resource-limited settings.[7] Therefore, novel sensing methods or devices detecting a low amount of proteins directly from a complex mixture such as human serum have the potential to advance conventional diagnostic techniques to further levels.

Over the years, magnetic-based detection techniques have gained much attention as ideal candidates for biomarker analysis due to their contactless control in biological samples, ease of operation, low energy requirement, and simple design.[8−10] Magnetic-based protein detection technologies have focused on the use of magnetic nanoparticles (MNPs), which are typically made of a magnetic core (e.g., Fe_3O_4 and γFe_2O_3) and a surrounding shell (e.g., dextran and silica).[11] Labeling of biological particles lacking magnetic property in nature with MNPs makes them susceptible to the magnetic field so they can be controlled by a simple magnet. In magnetic-based biosensing applications, MNPs can be exploited as magnetic labels, assay substrates on which the protein of interest is captured, or both.[8] In several studies,[12−15] these particles allowed highly sensitive detection of proteins using microfluidic devices. Since these studies require precise control of microfluidic flow rates and sophisticated experimental schemes, they could not offer easy-to-use and low-cost detection schemes.

Magnetic levitation, which is levitating objects under an inhomogeneous magnetic field based on the balance of magnetic and buoyancy forces, has inspired many applications, including sorting numerous materials,[16−18] the association of proteins and ligands,[19−22] cell measurement and detection,[23−29] 3D assembly of living cells,[30−32] and biomarker detection.[33,34] Lately, this technology has emerged to provide

Received: June 10, 2020
Accepted: August 19, 2020
Published: August 19, 2020

https://dx.doi.org/10.1021/acs.analchem.0c02479
Anal. Chem. 2020, 92, 12556−12563

high-throughput,[35] compact, and portable analysis of microparticle and cell densities.[28,29,36−38] Fundamentals and applications of magnetic levitation are well documented in recent review articles.[39−41]

A simply -designed magnetic levitation setup consists of two magnets whose same poles face each other. A particle suspended in a paramagnetic liquid is levitated between these magnets at an equilibrium position determined by its density and magnetic susceptibility relative to the surrounding liquid. Briefly, measuring the levitation height of an object reveals the density and magnetic susceptibility. So far, density change regarding the binding of proteins onto the beads is measured by monitoring the levitation height change in the magnetic levitation system and correlating to the amount of proteins bound onto the beads.[21,27,33,34] One of those is a multiplex detection of antibodies against syphilis and hepatitis C by observing the height change of levitating polystyrene beads upon binding of antibodies and subsequent deposition of metal nanoparticles.[33] Recently, the levitation height of two different-density polymethylmethacrylate microspheres has been tracked for the quantification of interleukin-6 (IL-6).[27] These antibody-coated microspheres conjugate in the presence of IL-6 and reach a density value between those of two types of microspheres. The technique can detect 10 pg/mL (corresponds to ∼0.5 pM) of IL-6 in phosphate-buffered saline (PBS) samples. Moreover, Chagas disease-related anti-*Trypanosoma cruzi* antibodies in blood samples were quantified with a detection limit of 5 μg/mL (corresponds to ∼30 μM).[34]

Here, apart from density-based techniques using the magnetic levitation principle, we present a magnetic susceptibility-based protein detection method using polymer microspheres as mobile assay surfaces and MNPs as labels. Labeling protein conjugated-polymer microspheres with MNPs changed the magnetic susceptibility of the conjugate, and in the magnetic levitation system, the equilibrium height of the complex was significantly altered compared to no protein-conjugated microspheres. Approximately 110 fg/mL (∼1.6 fM) biotinylated bovine serum albumin (b-BSA) could be detected in serum. With the developed sandwich immunoassay, detection limits for mouse immunoglobulin G (IgG) in pure buffer and serum were 1.5 ng/mL (∼10 pM) and >10 ng/mL, respectively. The assay required 200 μL of sample and reasonably short analysis time (∼50 min for assay preparation steps off the platform and ∼30 min for levitation on the platform). The results suggested that magnetic levitation-based assays hold a great promise for sensitive and rapid protein analysis in serum samples.

EXPERIMENTAL SECTION

Experimental Setup. The protein assay was performed in a magnetic levitation platform composed of (i) two magnets (N52-grade neodymium, 50 mm length × 2 mm width × 5 mm height, supermagnete.de) with polarization through their heights, (ii) two mirrors (1/2″ square protected aluminum mirror, 3.2 mm-thick, Thorlabs) tilted at 45° to monitor the channel along its height using an inverted microscope, and (iii) a glass microcapillary channel (50 mm length × 1 mm width × 1 mm height, vitrocom.com) with a wall thickness of 0.2 mm placed between the magnets (Figure S1). The glass capillary has a tolerance of ±10% for its inner dimensions. The parts of the platform were assembled in a 3D-printed body, which was produced by stereolithography using photoreactive resin "Clear v2 FLGPCL02" at a resolution of 25 μm (Formlabs, Form2 3D printer) (Figure S2).

Design and Characterization of the Magnetic Levitation-Based Protein Assay Using b-BSA. The assay for b-BSA detection included streptavidin-coated fluorescent polystyrene microspheres (s-PMS) (Streptavidin Fluoresbrite HG 6 μm polystyrene beads, Polysciences Inc.), streptavidin coated-magnetic nanoparticles (s-MNP) (MACS streptavidin-coupled microbeads, 50 nm, #130-048-102, Miltenyi Biotec), and b-BSA (Sigma-Aldrich, #A8549-10MG) as a model protein. Gd-BT-DO3A (Gadavist, gadobutrol (Gd^{3+})), which is a nonionic paramagnetic medium with weak protein binding properties,[42] was used to increase the magnetic susceptibility difference between microspheres and the medium. Cell viability tests also revealed that this medium showed good biocompatibility up to 200 mM concentration levels.[9,31]

In brief, the protein detection protocol starts with the incubation of s-PMS at two different concentrations (i.e., 10^5 or 10^6 particles/mL) with the sample solution (200 μL) for 30 min on a vortex mixer. As a sample, b-BSA was spiked either in PBS (Gibco, pH = 7.4) or in dialyzed fetal serum albumin (FBS) (Sigma-Aldrich). Prepared FBS samples were diluted either 1:10 (v/v) with PBS containing 1% (v/v) Tween 20 or 1:1 (v/v) with 1% (w/v) Pluronic F127 (Sigma-Aldrich). Then, the mixture was centrifugated at 13,500 rpm (DAIHAN Scientific CF-10) for 5 min and the supernatant was discarded. Finally, b-BSA-bound s-PMS were resuspended in 200 μL of a levitation buffer (i.e., either PBS (pH = 7.4) containing 1% (v/v) Tween or 1% (w/v) Pluronic F-127) and incubated with 1 μL of s-MNP stock solution for 15 min. After it was mixed with 1 M Gd^{3+} stock solution (with volumes of 0.4, 1.2, 2.4, and 3.6 μL to get 10, 30, 60, and 90 mM Gd^{3+} in the final solution, respectively), the mixture (40 μL) was loaded into the microcapillary channel using an automatic micropipette. For each experiment, a new microcapillary treated with an air plasma for 4 min at 0.5 mbar and 100 W (Diener plasma cleaner) was used. After sample loading, one end of the microcapillary channel was sealed by immersing it into the Critoseal (Leica Microsystems, Germany). Then, the capillary was inserted into the magnetic levitation platform. The center part of the channel was monitored under an inverted microscope (Zeiss Axio Observer Z1, 5× objective) equipped with a camera (Zeiss AxioCam ICm1). A single micrograph of the microcapillary was used to analyze microsphere positions for each experiment. Distance measurements on the images were conducted using the Image J Software (Supporting Information, Table S1 and Figure S3). In a single micrograph, 100−120 microspheres could be analyzed at a concentration of 10^6 microspheres/mL.

Application of the Assay for the Measurement of Immunoglobulin G Levels. The proof of concept developed for b-BSA was tested for the detection of mouse IgG (Sigma-Aldrich, I5381) spiked in buffer and serum as the target protein biomarker. Biofunctionalization of streptavidin polymer microspheres and magnetic nanoparticles with biotinylated goat anti-mouse IgG (Sigma-Aldrich, B7264) is presented in the Supporting Information. All IgG experiments were conducted in PBS and FBS diluted 1:1 with PBS (pH = 7.4) containing 1% (w/v) Pluronic F-127 and 1% (w/v) BSA (Sigma-Aldrich) (Supporting Information). The incubation and levitation procedures performed in b-BSA tests were also applied for IgG (Supporting Information). On the other hand,

https://dx.doi.org/10.1021/acs.analchem.0c02479
Anal. Chem. 2020, 92, 12556−12563

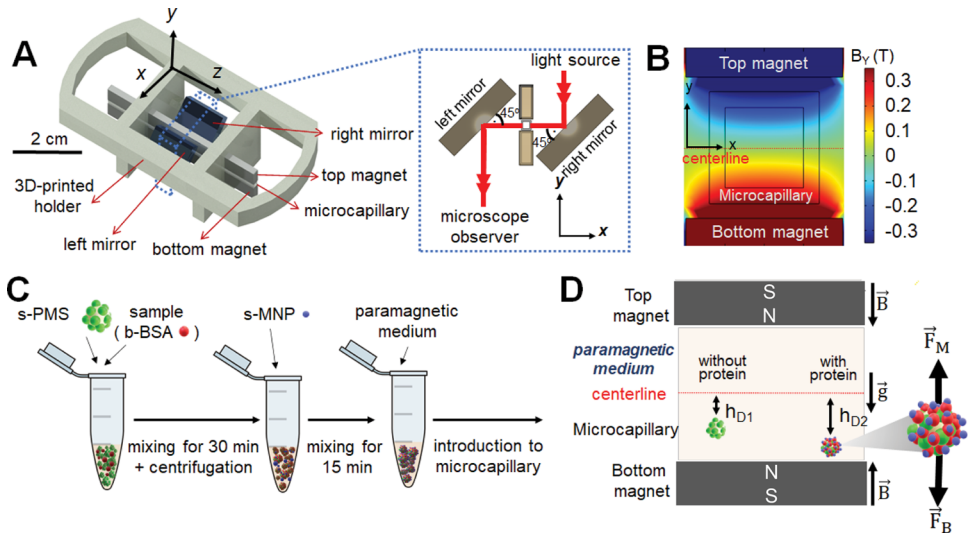

Figure 1. Principles of the magnetic levitation-based protein assay. (A) Illustration of the setup. A 3D-printed holder is used to assemble mirrors, magnets, and a glass microcapillary. Two tilted side mirrors are attached onto the 3D-printed holder to monitor inside the capillary. (B) Magnetic induction in the y direction (B_y). Magnets are separated 1800 μm from each other, and the microcapillary with a channel height of 1000 μm and a channel wall thickness of 200 μm is placed between the magnets. (C) Schematic representation of offline incubation steps. (D) Schematic representation of the protein detection principle. Due to magnetic induction ($\vec{B}$) and gravity ($\vec{g}$), microspheres inside the capillary channel levitate where the magnetic force ($\vec{F}_M$) is balanced by the buoyancy force ($\vec{F}_B$). Upon binding of protein (b-BSA) and s-MNP onto the s-PMS, the complex gains magnetic susceptibility and levitates significantly different than the no-protein condition (reference test). h_D represents the deviation distance of the microspheres from the centerline plane.

the concentrations of MNPs were optimized to enhance binding efficiency (Supporting Information, Figure S4).

Statistical Analysis. All experiments were repeated three times using a new capillary channel for each experiment, and data are presented as mean ± standard deviation (SD) from the mean values of triplicates. Statistical significance was determined by one-way analysis of variance (ANOVA) corrected for multiple comparisons and t test with Welch's correction. Coefficient of variation (CV) (%) was calculated as (standard deviation of population/mean of the population) × 100. Statistical outliers in data were detected and removed under the integrated robust regression and outlier removal (ROUT) method[43] for different maximum desired false discovery rate (Q) values (i.e., 0.5, 1, 2, and 5%) for CV (%)-based analysis. These analyses were conducted using GraphPad Prism (version 6.0). The mean values of experimental data were fitted into linear curves (i.e., semilog lines) to obtain standard equations for deviation height/CV versus protein concentration.

RESULTS AND DISCUSSION

The magnetic levitation platform includes two permanent neodymium magnets at the opposing configuration (i.e., same magnetic poles face each other), a glass microcapillary channel inserted between the magnets (50 mm length × 1 mm width × 1 mm height), two mirrors tilted at 45° to monitor inside the channel using an inverted microscope, and a 3D-printed holder to maintain these pieces (Figure 1A). In this platform, magnetic induction ($\vec{B}$) reaches its maxima near the magnets and its minima at the midpoint between the magnets (Figure 1B). Our magnet configuration creates a linear magnetic induction in the y direction (B_y) in the interspace between the magnets separated by 1.8 mm (Figure S5). When diamagnetic microspheres are spiked in a nonionic paramagnetic medium, they come into an equilibrium position along with the channel height and levitate where the magnetic force ($\vec{F}_M$) is counterbalanced with the buoyancy force ($\vec{F}_B$).[31] Under the same magnetic field conditions, the steady-state levitation height of a microsphere depends purely on the magnetic susceptibility (χ) and density (ρ) difference between the microsphere and paramagnetic medium. For instance, if the microspheres have high magnetic susceptibility or density (e.g., magnetic nanoparticles), they levitate close to the magnets whereas diamagnetic particles (e.g., polymer microspheres) are repelled by the applied magnetic field and levitate close to the midpoint between the magnets (Supporting Information, Figure S6).

Characterization of Magnetic Levitation-Based Protein Measurement. Our method detects b-BSA by monitoring levitation heights of s-PMS. The deviation height of microspheres (h_D) is calculated as the distance of microspheres from the centerline plane between magnets in the presence of b-BSA and s-MNP. In the assay (Figure 1C), b-BSA molecules are captured on s-PMS surfaces, and the captured b-BSA are labeled with s-MNP due to strong molecular affinity between streptavidin and biotin molecules (K_a = ~2.5 × 10^{13} M^{-1}).[44] These conjugations alter the net magnetic susceptibility and density of s-PMS, and so they significantly change the deviation height of s-PMS compared to s-PMS without b-BSA (Figure 1D). Our assay monitors two parameters for protein detection: (i) average deviation height of microspheres labeled with magnetic nanoparticles and (ii) deviation height distribution of microspheres.

Modeling and Design of Assay Protocol. We tested the levitation profile of s-PMS spiked in 30 mM Gd^{3+} with (i) no b-BSA, (ii) 1.05 ng/mL b-BSA, and (iii) 1.05 ng/mL b-BSA and s-MNP (Figure 2A). The significant change in levitation of s-PMS occurred in the presence of s-MNP (Figure 2B) similar to the simulation results (Supporting Information, Figures S6 and S7. Most of proteins are diamagnetic in nature and have very small magnetic susceptibility (e.g., χ_{BSA}: -0.826×10^{-6} (CGS units)[45] and e.g., χ_{water}: -0.719×10^{-6} (CGS units)[46]).

https://dx.doi.org/10.1021/acs.analchem.0c02479
Anal. Chem. 2020, 92, 12556−12563

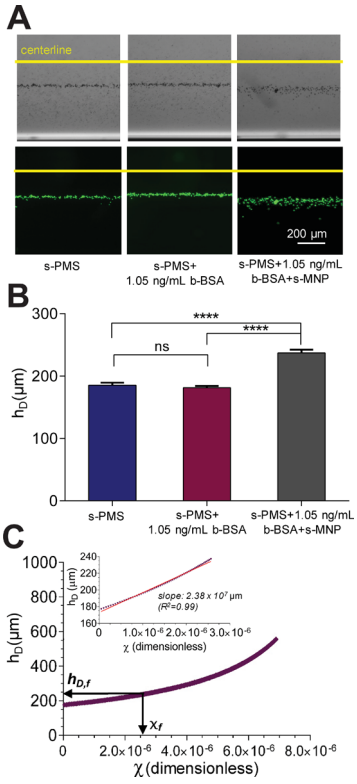

Figure 2. Sensitivity of the protein assay in the presence and absence of magnetic nanoparticles for detection of 1.05 ng/mL b-BSA. (A) Bright-field and fluorescent microscopy images of s-PMS after 30 min of levitation in the 30 mM Gd^{3+}-based paramagnetic medium. Micrographs correspond to reference (no b-BSA), s-PMS with 1.05 ng/mL b-BSA, and s-PMS with 1.05 ng/mL b-BSA and s-MNP experiments. (B) Quantitative deviation height analysis of microspheres shown in (A). Data are presented as mean deviation height ± SD. Data are compared with each other using one-way ANOVA. ****: $P < 0.0001$ and ns: not significant. (C) Magnetic susceptibility versus deviation height simulation for s-PMS. The final magnetic susceptibility (χ_f) of s-PMS in the presence of 1.05 ng/mL b-BSA and s-MNPs can be determined from the distinct deviation height ($h_{D,f}$) of s-PMS. Zoomed plot and linear fit to the data with a coefficient of determination (R^2) are shown in the figure.

Hence, there was no significant change in the density and magnetic susceptibility of s-PMS upon the binding of b-BSA, and consequently, the deviation height of s-PMS was not altered. On the other hand, s-MNP attached onto the s-PMS and BSA complex changed the overall magnetic susceptibility (χ_p) of the complex and set a new levitation height for s-PMS, which is closed to the bottom magnet. Later, the magnetic susceptibility change due to the attachment of 1.05 ng/mL b-BSA was calculated to be 2.7×10^{-6} (SI units) from Figure 2C by fitting the deviation height versus magnetic susceptibility data shown in Figure S7.

In routine operations, superconducting quantum interference device[47] magnetometry, vibrating-sample magnetometer,[48] and nuclear magnetic resonance[49] are widely used techniques for sensitive magnetic susceptibility measurements of materials. However, they include a hard-to operate and expensive scheme that is not optimized for single-particle measurements. To overcome these limitations, magnetophoretic motion of particles in a nonhomogeneous magnetic field has been used for measuring volumetric susceptibilities of both nonlabeled cells ($\chi_{\text{HeLa tumor cells}}$: -0.5136×10^{-6} (CGS units))[50] and labeled cells ($\chi_{\text{yeast, liver, and carcinoma cells}}$: $13-20 \times 10^{-6}$ (SI units)).[51] In this study, we used a magnetic levitation strategy to measure target proteins captured on microspheres with a change in the magnetic susceptibility of microspheres. Our method can distinguish a volumetric magnetic susceptibility of a single microsphere with a resolution of 4.2×10^{-8} (SI units) per 1 μm deviation height change in a 30 mM Gd^{3+}-based paramagnetic liquid (Figure 2C).

Levitation of s-PMS in the Presence of b-BSA Spiked in PBS. Detection of b-BSA with the presented assay method was conducted in 30, 60, and 90 mM Gd^{3+}. For protein detection experiments in different Gd^{3+} concentrations, the levitation was conducted for 30 min to ensure steady-state deviation height profiles (Supplementary Information, Figure S8). The average deviation heights of s-PMS for various b-BSA concentrations are shown in Figure 3. The points including the

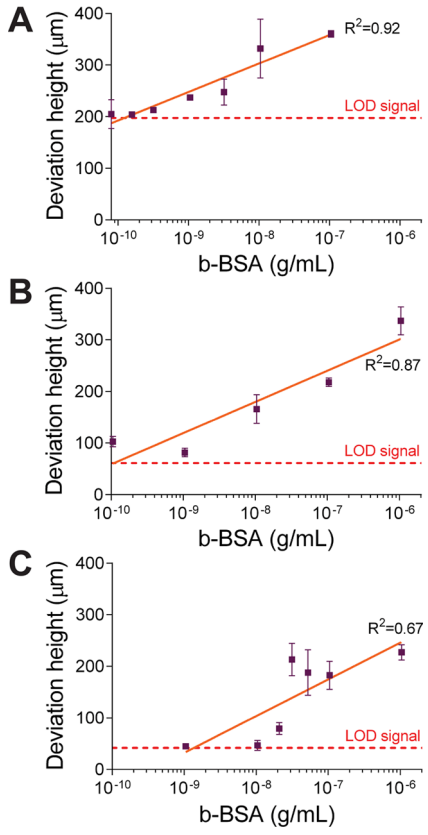

Figure 3. Levitation of s-PMS in b-BSA-spiked PBS samples. Deviation heights with (A) 30 mM, (B) 60 mM, and (C) 90 mM Gd^{3+}-based paramagnetic medium are presented. Data are shown as mean of three replicates with error bars (±SD). Linear fits to the data with coefficient of determination (R^2) are shown as solid lines.

reference condition (no b-BSA) are also presented in Figure S9. Limit of detection (LOD) signal was calculated as adding three standard deviations to the mean of reference signal (0 g/mL b-BSA).[52] Experimental results were fitted to a linear curve (Supporting Information, Figure S10). LOD concentration values were calculated as the intersection of these linear curves and the LOD signal. LOD values of >0.1 ng/mL were obtained in 30 mM and 60 mM Gd^{3+} solutions for b-BSA, whereas a >1 ng/mL LOD value was reached in 90 mM Gd^{3+} solutions. As shown in simulations (Figure S7), experimental results revealed that the detection sensitivity of the assay was

https://dx.doi.org/10.1021/acs.analchem.0c02479
Anal. Chem. 2020, 92, 12556−12563

improved with the decrease in Gd^{3+} concentration. The LOD value in PBS experiments using 30 mM Gd^{3+} (i.e., 0.12 ng/mL, ~2pM) requires ~1.0×10^4 b-BSA available molecules per microspheres in the solution. This corresponds to a 1×10^{-6} increase in the average magnetic susceptibility of the microspheres (Figure 2C), which is due to the attachment of more than 1.2×10^3 s-MNPs (Figure S7) per microspheres. Since microspheres started to reach the boundary of the capillary channel for 1 μg/mL b-BSA at 30 mM Gd^{3+}, deviation height values of microspheres would be saturated beyond this concentration.

Levitation of s-PMS in the Presence of b-BSA Spiked in FBS. Direct examination of biological molecules in blood serum of a patient is of great importance in diagnostic assay development strategies. In this regard, s-PMS and s-MNP were suspended in FBS without b-BSA and used as a reference test first. However, all s-PMSs were collected at the bottom of the capillary, probably due to the nonspecific adsorption of serum proteins and s-MNP onto the s-PMSs and causing microspheres to settle down to the bottom of the channel (Figure S11). To eliminate nonspecific adsorption of proteins, we used Tween 20 and Pluronic F-127 as nonionic surfactants.[53] We used PBS with 1% (v/v) Tween 20 solution (PBST) and PBS with 1% (w/v) Pluronic F-127 (PBSP) to dilute the FBS sample. For 1:1 (v/v) dilution of sample solution with PBST (1%) buffer, still no microsphere was observed in the glass microcapillary during the levitation, probably due to the continuing effect of nonspecific bindings. Later, the dilution ratio was increased to 1:10 (v/v) and microspheres could be levitated in the glass capillary. In the case of PBSP (1%), a 1:1 (v/v) ratio sample dilution worked for microspheres. Then, we tested the detection capacity of the magnetic levitation-based assay in the serum sample composed of FBS spiked with b-BSA. For b-BSA-spiked FBS tests, the sample was diluted with either 1:10 (v/v) using PBST or 1:1 (v/v) using PBSP. Experiments conducted with the 30 mM Gd^{3+}-based levitation medium revealed that deviation heights of s-PMS increased with b-BSA concentration and an LOD value of >1 ng/mL was obtained for b-BSA in FBS using both PBST and PBSP dilutions (Figure 4A,B). However, s-PMSs were less dispersed in the capillary channel with PBSP dilution than in that with PBST dilution (Figure S12) for the reference test.

We also analyzed the distribution profile of s-PMS for different b-BSA (Supporting Information, Figures S13–S18) since not all microspheres would end up with the attachment of the same number of magnetic nanoparticles due to the differences in their binding capacities. CV (%) statistically includes the relative dispersion of data points around the mean value. Because of that, we incorporated CV (%) into our analysis as an indicator of s-PMS distribution within the channel. s-PMS with b-BSA showed a more distributed deviation height profile within the microcapillary channel compared to the s-PMS without b-BSA (Figure S19). However, the average deviation height-based analysis did not include this distribution. Due the distributed profile of s-PMS, the change in CV (%) was greater than the change in average deviation height in the presence of b-BSA (Figure S20). As shown in Figure S21, there was a high distribution in the s-PMS profile for reference tests (CV ≅ 14%) using PBST dilution. On the other hand, for the dilution with Pluronic, s-PMSs in reference tests were not widely distributed (CV ≅ 7%). Hence, in our assay protocol, Pluronic in dilution buffer could eliminate better nonspecific bindings on s-PMS surfaces

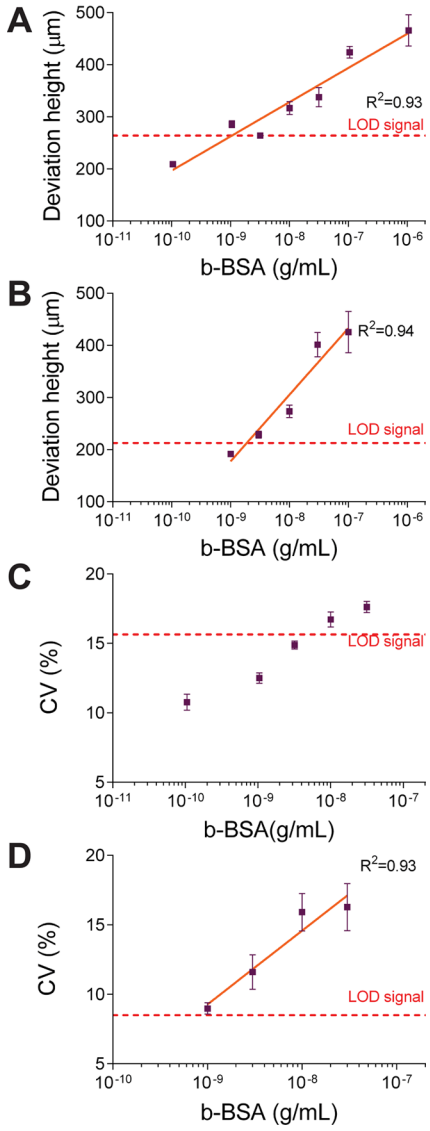

Figure 4. Levitation of s-PMS in b-BSA-spiked FBS samples under 30 mM Gd^{3+}-based levitation medium. The FBS samples were diluted using either PBST or PBSP. (A, B) Deviation height analyses of the sample diluted with PBST and PBSP, respectively. (C, D) CV (%) analyses of the deviation height profiles for PBST and PBSP dilutions, respectively. Data are shown as mean of three replicates with error bars (±SD). Linear fits to the data with coefficient of determination (R^2) are shown as solid lines.

than Tween. CV analysis revealed that detectable b-BSA concentrations could be slightly improved only for the experiments conducted with Pluronic (Figure 4C,D). This approach reduced the LOD down to sub ng/mL levels for b-BSA in FBS samples diluted 1:1 (v/v) with Pluronic. However, it should be noted that CV (%) of s-PMS is influenced by the number of analyzed particles. Therefore, s-PMS number in the channel should be kept constant in experiments.

We used 10-fold diluted s-PMS in order to improve the detection sensitivity in serum by increasing the number of target proteins per microsphere. Hence, much more b-BSA molecules and s-MNP labels would be concentrated on s-PMS for the same b-BSA concentration levels used in previous experiments. Experiments revealed that the LOD reached down to ~110 fg/mL for b-BSA in the serum sample diluted

https://dx.doi.org/10.1021/acs.analchem.0c02479
Anal. Chem. 2020, 92, 12556−12563

1:1 with PBSP (Figure 5 and Figure S22). However, the standard deviation increased between the repeats because of the low number of microspheres.

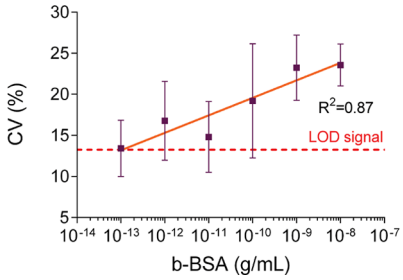

Figure 5. CV (%) analysis of the deviation height profiles of diluted s-PMS for different concentrations of b-BSA-spiked FBS sample prepared in PBSP. Data collected using the 30 mM Gd^{3+}-based levitation medium are shown as mean of three replicates with error bars (±SD). A linear fit to the data with a coefficient of determination (R^2) is shown as a solid line.

Detection of Immunoglobulin G as a Biomarker in Pure and Complex Media. Lastly, we applied a sandwich immunoassay on the polymer microspheres for detection of a serological biomarker. We chose IgG as the target biomarker to validate our method since IgG levels in blood are indicators of neutralization of toxins and pathogens[54] and autoimmune diseases.[55] The normal concentrations of total IgG in human blood range between 8−16 mg/mL[56] and discrepancies in total IgG levels in blood relate to serious health problems. For instance, in hypogammaglobulinemia, the IgG levels are significantly reduced.[57] On the other hand, elevated levels of IgG may be the signatures of cancer[58] or long-term infections such as HIV.[59] Moreover, antigen-specific IgG tests possess a very critical role in the conformation of viral infections such as severe acute respiratory syndrome coronavirus 2 (SARS-CoV-2) in which specific IgG concentration peaks at 16.47 μg/mL after the onset of the illness and remains at 11.4 μg/mL until 31−41 days.[60]

Microspheres and magnetic nanoparticles covered with biotinylated anti-mouse IgG antibodies were used to detect mouse IgG spiked in buffer and serum by monitoring deviation heights of microspheres (Figure 6). In PBS, the LOD value was determined as 1.5 ng/mL (∼10 pM) (Figure 6A) whereas in FBS, a higher concentration (>10 ng/mL) was detectable with CV analysis (Figure 6B). A similar LOD was observed in terms of deviation height analysis (Figure S23). The results revealed that LOD values increased for IgG compared to those for b-BSA. This could be due to the fact that b-BSA used in this study contains multiple binding sites (i.e., 8−16 mol biotin per mol BSA) for binding onto the s-PMS and s-MNP. Moreover, the streptavidin−biotin interaction has a 10^3−10^6 times higher affinity than an antibody−antigen formation and is not easily disturbed by assay manipulations such as washing steps.[61] In addition, the increase in LOD for IgG could be due to the lowered number of available target binding sites on particles since not all streptavidin molecules on their surface would be functionalized with the well-oriented biotinylated antibody. This can be eliminated by immobilizing a capture antibody covalently onto a preactivated solid phase, instead of using the streptavidin−biotin system. It is a complex method but may improve antibody density on the surface.[62]

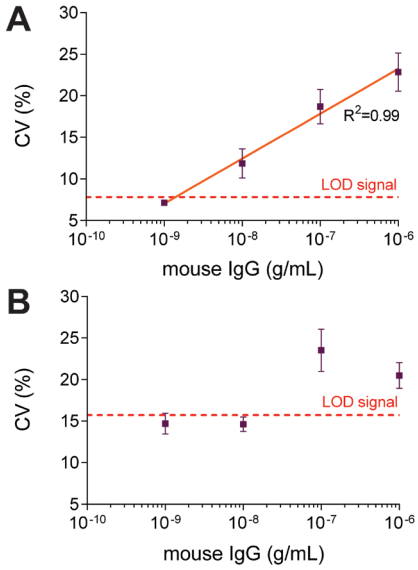

Figure 6. CV (%) analyses of the anti-mouse IgG microspheres for different concentrations of mouse IgG spiked in (A) PBS and (B) FBS. Data collected using the 30 mM Gd^{3+}-based levitation medium are shown as mean of three replicates with error bars (±SD). A linear fit to the data with a coefficient of determination (R^2) is shown as a solid line.

Magnetic Levitation-Based Protein Detection Methods. Magnetic levitation technology has been exploited to detect different proteins. Target proteins, sample volume, detection limits, assay time, and detection principle of those studies are summarized in Table S2. So far, the detection efforts have been based on density changes of microparticles upon binding of target molecules. Our study is novel in that it has proved the applicability of magnetic susceptibility-based protein detection under magnetic levitation offering notable protein detection levels of ∼110 fg/mL (∼1.6 fM) in serum samples and could improve the detection sensitivity of magnetic levitation technology further. Since biological samples mostly have weak magnetic signals,[63] the measurement based on magnetic susceptibility changes can also be used to detect many other clinically important biomolecules.

Compared to the detection limits (>100 pg/mL) and assay time (>360 min) of conventional ELISA,[64] our magnetic susceptibility-based protein assay provided low detection limits with a reasonable analysis time (∼80 min). The protein analysis with the presented strategy was conducted directly on a simple bright-field microscope with a more straightforward method that does not require complex instrumentation, numerous washing, and incubation steps unlike conventional ELISA. Moreover, magnetic nanoparticles could be adopted in ultrasensitive and automated on-chip protein analysis platforms.[15,65] For a remote and portable protein analysis, this assay could be adopted to low-cost and portable imaging systems such as cellular phones,[27] lensless holographic microscopy systems,[66,67] and self-contained and handheld magnetic levitation devices.[68,69] In addition, integration of the assay into flow-assisted magnetic levitation devices[70] could enable analyzing higher sample sizes and hence increasing the sensitivity of protein detection.

Our proposed detection method uses centrifugation to eliminate sample matrices. Hence, the analysis is independent from the variabilities coming from the real sample

https://dx.doi.org/10.1021/acs.analchem.0c02479
Anal. Chem. 2020, 92, 12556−12563

composition, such as viscosity and density. Even if there are some residues of detected molecules left in the paramagnetic medium with a density of 1.016 g/mL, their effect on the medium density is very low since low concentrations of molecules (≤1 μg/mL) were used in our study. Moreover, if the sample medium (i.e., FBS with a density of 1.025 g/mL[23]) remains in the paramagnetic medium, its effect should also be observed in the reference tests (i.e., without the target molecule). The effect of centrifugation on the levitation height of microspheres was not observed also (Figure S24). In addition, the aggregation of the microspheres does not alter the net levitation height of microspheres since the levitation height is independent from the volume of the microspheres (Figure S6). It is also known that the magnetic levitation profile is not significantly affected by mild temperature changes (28−36 °C).[31] Considering all, we believe that the method shown here could provide consistent readouts in the field. For more sensitive protein detection, MNP labels with higher susceptibility can be easily adapted in the presented method so that microspheres can deviate more under the same magnetic field and create a significant levitation height change in the presence of ultralow protein concentrations. By changing the surface properties of the particles, the unspecific adsorption can be reduced in complex media such as blood plasma, and the sensitivity of the assay can be further increased.[71]

CONCLUSIONS

In this study, we demonstrated a new method of using diamagnetic microspheres as mobile assay substrates to catch the target protein and magnetic nanoparticles as labels to increase the magnetic susceptibility of protein-conjugated microspheres. The increase in the magnetic susceptibility results in a significant deviation of microsphere−protein conjugates from the centerline of the two magnets compared to microspheres containing no protein. While other magnetic levitation-based protein detection methods focus on density changes of particles due to binding of target analytes, here, we propose a method that utilizes minute magnetic susceptibility changes upon labeling the target with magnetic nanoparticles. Hence, apart from protein detection, the method developed here could be used to estimate the magnetic susceptibility changes of particles with a resolution of 4.2×10^{-8}. Moreover, the assay platform does not depend on electric power to operate, and it offers a plain and low-cost design (<$30) that can be mounted easily to a regular microscope for protein measurements. The presented protein detection assay could also be adopted for the detection of any other target molecule using polymeric and magnetic micro/nanoparticles decorated with specific recognition molecules against the target molecule. This could enable a broad range of applications in the field of environmental inspection, food and water safety, drug screening tests, and medical diagnosis.

ASSOCIATED CONTENT

Supporting Information

The Supporting Information is available free of charge at https://pubs.acs.org/doi/10.1021/acs.analchem.0c02479.

Figures S1−S24 and Tables S1 and S2; calculation of deviation heights of microspheres; biofunctionalization and levitation of particles for immunoglobulin G detection; modeling and simulation of the system; levitation profile of s-PMS in paramagnetic medium; fitting of experimental data; and ROUT analysis for elimination of outlier microspheres (PDF)

AUTHOR INFORMATION

Corresponding Author

H. Cumhur Tekin − *Department of Bioengineering, Izmir Institute of Technology, Izmir 35430, Turkey; METU MEMS Center, Ankara 06520, Turkey;* orcid.org/0000-0002-5758-5439; Email: cumhurtekin@iyte.edu.tr

Author

Sena Yaman − *Department of Bioengineering, Izmir Institute of Technology, Izmir 35430, Turkey*

Complete contact information is available at: https://pubs.acs.org/10.1021/acs.analchem.0c02479

Author Contributions

All authors contributed equally to this manuscript.

Notes

The authors declare no competing financial interest.

ACKNOWLEDGMENTS

Financial support from The Scientific and Technological Research Council of Turkey (116M298) and Izmir Institute of Technology (2016IYTE68-BAP) are gratefully acknowledged. The authors would like to thank Engin Ozcivici, PhD, from the Department of Bioengineering, Izmir Institute of Technology, for helpful discussions and suggestions. The authors would also like to thank Katherine Willcox Ozsari from Izmir Institute of Technology for proofreading the manuscript.

REFERENCES

(1) Kristiansen, G. *Histopathology* **2012**, *60*, 125−141.
(2) Tran, H. T.; Liu, Y.; Zurita, A. J.; Lin, Y.; Baker-Neblett, K. L.; Martin, A. M.; Figlin, R. A.; Hutson, T. E.; Sternberg, C. N.; Amado, R. G.; Pandite, L. N.; Heymach, J. V. *The Lancet. Oncology* **2012**, *13*, 827−837.
(3) Lam, S. W.; Jimenez, C. R.; Boven, E. *Cancer Treat. Rev.* **2014**, *40*, 129−138.
(4) Signorelli, S. S.; Fiore, V.; Malaponte, G. *Int. J. Mol. Med.* **2014**, *33*, 777−783.
(5) Blennow, K.; Zetterberg, H. *Front. Neurosci.* **2015**, *9*, 345.
(6) Araujo, M.; Doi, S. Q. *Front. Med.* **2017**, *4*, 168−168.
(7) Sharma, S.; Zapatero-Rodríguez, J.; Estrela, P.; O'Kennedy, R. *Biosensors* **2015**, *5*, 577−601.
(8) Tekin, H. C.; Gijs, M. A. M. *Lab Chip* **2013**, *13*, 4711−4739.
(9) Yaman, S.; Anil-Inevi, M.; Ozcivici, E.; Tekin, H. C. *Front. Bioeng. Biotech.* **2018**, *6*, 192.
(10) Alnaimat, F.; Dagher, S.; Mathew, B.; Hilal-Alnqbi, A.; Khashan, S. *Chem. Rec.* **2018**, *18*, 1596−1612.
(11) Jamshaid, T.; Neto, E. T. T.; Eissa, M. M.; Zine, N.; Kunita, M. H.; El-Salhi, A. E.; Elaissari, A. *TrAC - Trend. Anal. Chem.* **2016**, *79*, 344−362.
(12) Jin, Z.; Hahn, Y. K.; Oh, E.; Kim, Y.-P.; Park, J.-K.; Moon, S. H.; Jang, J.-T.; Cheon, J.; Kim, H.-S. *Small* **2009**, *5*, 2243−2246.
(13) Hall, D. A.; Gaster, R. S.; Lin, T.; Osterfeld, S. J.; Han, S.; Murmann, B.; Wang, S. X. *Biosens. Bioelectron.* **2010**, *25*, 2051−2057.
(14) Proczek, G.; Gassner, A.-L.; Busnel, J.-M.; Girault, H. H. *Anal. Bioanal. Chem.* **2012**, *402*, 2645−2653.
(15) Tekin, H. C.; Cornaglia, M.; Gijs, M. A. M. *Lab Chip* **2013**, *13*, 1053−1059.
(16) Andres, U. *Magnetohydrodynamic and Magnetohydrostatic methods of mineral separation*; Wiley: New York, 1976.
(17) Nemiroski, A.; Soh, S.; Kwok, S. W.; Yu, H.-D.; Whitesides, G. M. *J. Am. Chem. Soc.* **2016**, *138*, 1252−1257.

(18) Mirica, K. A.; Phillips, S. T.; Mace, C. R.; Whitesides, G. M. *J. Agric. Food Chem.* **2010**, *58*, 6565−6569.
(19) Mirica, K. A.; Phillips, S. T.; Shevkoplyas, S. S.; Whitesides, G. M. *J. Am. Chem. Soc.* **2008**, *130*, 17678−17680.
(20) Benz, L.; Cesafsky, K. E.; Le, T.; Park, A.; Malicky, D. *J. Chem. Educ.* **2012**, *89*, 776−779.
(21) Shapiro, N. D.; Mirica, K. A.; Soh, S.; Phillips, S. T.; Taran, O.; Mace, C. R.; Shevkoplyas, S. S.; Whitesides, G. M. *J. Am. Chem. Soc.* **2012**, *134*, 5637−5646.
(22) Shapiro, N. D.; Soh, S.; Mirica, K. A.; Whitesides, G. M. *Anal. Chem.* **2012**, *84*, 6166−6172.
(23) Durmus, N. G.; Tekin, H. C.; Guven, S.; Sridhar, K.; Arslan Yildiz, A.; Calibasi, G.; Ghiran, I.; Davis, R. W.; Steinmetz, L. M.; Demirci, U. *Proc. Natl. Acad. Sci. U. S. A.* **2015**, *112*, E3661−E3668.
(24) Tasoglu, S.; Khoory, J. A.; Tekin, H. C.; Thomas, C.; Karnoub, A. E.; Ghiran, I. C.; Demirci, U. *Adv. Mater.* **2015**, *27*, 3901−3908.
(25) Andersen, M. S.; Lu, S.; Lopez, G. J.; Lassen, A. T.; Shapiro, N. I.; Ghiran, I. C. *Shock* **2019**, *51*, 147−152.
(26) Sarigil, O.; Anil-Inevi, M.; Yilmaz, E.; Mese, G.; Tekin, H. C.; Ozcivici, E. *Analyst* **2019**, *144*, 2942−2953.
(27) Andersen, M. S.; Howard, E.; Lu, S.; Richard, M.; Gregory, M.; Ogembo, G.; Mazor, O.; Gorelik, P.; Shapiro, N. I.; Sharda, A. V.; Ghiran, I. *Lab Chip* **2017**, *17*, 3462−3473.
(28) Knowlton, S. M.; Sencan, I.; Aytar, Y.; Khoory, J.; Heeney, M. M.; Ghiran, I. C.; Tasoglu, S. *Sci. Rep.* **2015**, *5*, 15022.
(29) Felton, E. J.; Velasquez, A.; Lu, S.; Murphy, R. O.; ElKhal, A.; Mazor, O.; Gorelik, P.; Sharda, A.; Ghiran, I. C. *Lab Chip* **2016**, *16*, 3286−3295.
(30) Haisler, W. L.; Timm, D. M.; Gage, J. A.; Tseng, H.; Killian, T. C.; Souza, G. R. *Nat. Protoc.* **2013**, *8*, 1940.
(31) Anil-Inevi, M.; Yaman, S.; Yildiz, A. A.; Mese, G.; Yalcin-Ozuysal, O.; Tekin, H. C.; Ozcivici, E. *Sci. Rep.* **2018**, *8*, 7239.
(32) Mishriki, S.; Abdel Fattah, A. R.; Kammann, T.; Sahu, R. P.; Geng, F.; Puri, I. K. *Research* **2019**, *2019*, 13.
(33) Subramaniam, A. B.; Gonidec, M.; Shapiro, N. D.; Kresse, K. M.; Whitesides, G. M. *Lab Chip* **2015**, *15*, 1009−1022.
(34) Castro, B.; de Medeiros, M. S.; Sadri, B.; Martinez, R. V. *Analyst* **2018**, *143*, 4379−4386.
(35) Ge, S.; Wang, Y.; Deshler, N. J.; Preston, D. J.; Whitesides, G. M. *J. Am. Chem. Soc.* **2018**, *140*, 7510−7518.
(36) Amin, R.; Knowlton, S.; Dupont, J.; Bergholz, J. S.; Joshi, A.; Hart, A.; Yenilmez, B.; Yu, C. H.; Wentworth, A.; Zhao, J. J.; Tasoglu, S. *J. 3D Print. Med.* **2017**, *1*, 155−164.
(37) Knowlton, S.; Joshi, A.; Syrrist, P.; Coskun, A. F.; Tasoglu, S. *Lab Chip* **2017**, *17*, 2839−2851.
(38) Knowlton, S.; Yu, C. H.; Jain, N.; Ghiran, I. C.; Tasoglu, S. *PLoS One* **2015**, *10*, e0134400−e0134400.
(39) Gao, Q.-H.; Zhang, W.-M.; Zou, H.-X.; Li, W.-B.; Yan, H.; Peng, Z.-K.; Meng, G. *Mater. Horiz.* **2019**, *6*, 1359−1379.
(40) Ge, S.; Nemiroski, A.; Mirica, K. A.; Mace, C. R.; Hennek, J. W.; Kumar, A. A.; Whitesides, G. M. *Angew. Chem., Int. Ed* **2020**, *59*, 2−48.
(41) Turker, E.; Arslan-Yildiz, A. *ACS Biomater. Sci. Eng.* **2018**, *4*, 787−799.
(42) Staks, T.; Schuhmann-Giampieri, G.; Frenzel, T.; Weinmann, H. J.; Lange, L.; Platzek, J. *Invest. radiol.* **1994**, *29*, 709−715.
(43) Motulsky, H. J.; Brown, R. E. *BMC Bioinf.* **2006**, *7*, 123.
(44) Deng, L.; Kitova, E. N.; Klassen, J. S. *J. Am. Soc. Mass Spectr.* **2012**, *24*, 49−56.
(45) Luo, J.; He, X.; Andre'd'Avignon, D.; Ackerman, J. J. H.; Yablonskiy, D. A. *J. Magn. Reson.* **2010**, *202*, 102−108.
(46) Spees, W. M.; Yablonskiy, D. A.; Oswood, M. C.; Ackerman, J. J. H. *Magn. Reson. Med.* **2001**, *45*, 533−542.
(47) Cukauskas, E. J.; Vincent, D. A.; Deaver, B. S., Jr. *Rev. Sci. Instrum.* **1974**, *45*, 1−6.
(48) Foner, S. *Rev. Sci. Instrum.* **1959**, *30*, 548−557.
(49) Frei, K.; Bernstein, H. J. *J. Chem. Phys.* **1962**, *37*, 1891−1892.
(50) Kashevskii, B. E.; Kashevskii, S. B.; Prokhorov, I. V.; Aleksandrova, E. N.; Istomin, Y. P. *Biophysics* **2006**, *51*, 902−907.
(51) Russell, A. P.; Evans, C. H.; Westcott, V. C. *Anal. Biochem.* **1987**, *164*, 181−189.
(52) Shrivastava, A.; Gupta, V. *Chron. Young Sci.* **2011**, *2*, 21−25.
(53) Boxshall, K.; Wu, M.-H.; Cui, Z.; Cui, Z.; Watts, J. F.; Baker, M. A. *Surf. Interface Anal.* **2006**, *38*, 198−201.
(54) Diem, S.; Fässler, M.; Bomze, D.; Ali, O. H.; Berner, F.; Niederer, R.; Hillmann, D.; Mangana, J.; Levesque, M. P.; Dummer, R.; Risch, L.; Recher, M.; Risch, M.; Flatz, L. *J. Immunother.* **2019**, *42*, 89−93.
(55) Haroun, M.; El-Sayed, M. M. *J. Clin. Biochem. Nutr.* **2007**, *40*, 56−61.
(56) Linder, V.; Verpoorte, E.; de Rooij, N. F.; Sigrist, H.; Thormann, W. *Electrophoresis* **2002**, *23*, 740−749.
(57) Pimenta, F. M. C. A.; Palma, S. M. U.; Constantino-Silva, R. N.; Grumach, A. S. *Braz. J. Med. Biol. Res.* **2019**, *52*, e8926−e8926.
(58) Qiu, X.; Zhu, X.; Zhang, L.; Mao, Y.; Zhang, J.; Hao, P.; Li, G.; Lv, P.; Li, Z.; Sun, X.; Wu, L.; Zheng, J.; Deng, Y.; Hou, C.; Tang, P.; Zhang, S.; Zhang, Y. *Cancer Res.* **2003**, *63*, 6488.
(59) McGowan, J. P.; Shah, S. S.; Small, C. B.; Klein, R. S.; Schnipper, S. M.; Chang, C. J.; Rosenstreich, D. L. *Med. Sci. Monit.* **2006**, *12*, Cr11−Cr16.
(60) Ma, H.; Zeng, W.; He, H.; Zhao, D.; Yang, Y.; Jiang, D.; Zhou, P.; Qi, Y.; He, W.; Zhao, C.; Yi, R.; Wang, X.; Wang, B.; Xu, Y.; Yang, Y.; Kombe Kombe, A. J.; Ding, C.; Xie, J.; Gao, Y.; Cheng, L.; et al. *medRxiv* **2020**, DOI: 10.1101/2020.04.17.20064907. 2020.2004.2017.20064907
(61) Diamandis, E. P.; Christopoulos, T. K. *Clin. Chem.* **1991**, *37*, 625−636.
(62) Welch, N. G.; Scoble, J. A.; Muir, B. W.; Pigram, P. J. *Biointerphases* **2017**, *12*, No. 02D301.
(63) Tao, Q.; Zhang, L.; Han, X.; Chen, H.; Ji, X.; Zhang, X. *Biophys. J.* **2020**, *118*, 578−585.
(64) Rissin, D. M.; Kan, C. W.; Campbell, T. G.; Howes, S. C.; Fournier, D. R.; Song, L.; Piech, T.; Patel, P. P.; Chang, L.; Rivnak, A. J.; Ferrell, E. P.; Randall, J. D.; Provuncher, G. K.; Walt, D. R.; Duffy, D. C. *Nat. Biotechnol.* **2010**, *28*, 595.
(65) Cornaglia, M.; Trouillon, R.; Tekin, H. C.; Lehnert, T.; Gijs, M. A. M. *Anal. Chem.* **2014**, *86*, 8213−8223.
(66) Delikoyun, K.; Yaman, S.; Tekin, H. C. Density-Based Separation of Microparticles Using Magnetic Levitation Technology Integrated on Lensless Holographic Microscopy Platform. In *2019 Innovations in Intelligent Systems and Applications Conference (ASYU)*; 2019, pp. 1−6.
(67) Sobieranski, A. C.; Inci, F.; Tekin, H. C.; Yuksekkaya, M.; Comunello, E.; Cobra, D.; von Wangenheim, A.; Demirci, U. *Light Sci. Appl.* **2015**, *4*, e346−e346.
(68) Yenilmez, B.; Knowlton, S.; Tasoglu, S. *Adv. Mater. Technol.* **2016**, *1*, 1600144.
(69) Yenilmez, B.; Knowlton, S.; Yu, C. H.; Heeney, M. M.; Tasoglu, S. *Adv. Mater. Technol.* **2016**, *1*, 1600100.
(70) Amin, R.; Knowlton, S.; Yenilmez, B.; Hart, A.; Joshi, A.; Tasoglu, S. *RSC Adv.* **2016**, *6*, 93922−93931.
(71) Lichtenberg, J. Y.; Ling, Y.; Kim, S. *Sensors* **2019**, *19*, 2488.

https://dx.doi.org/10.1021/acs.analchem.0c02479
Anal. Chem. 2020, 92, 12556−12563